Title: The SARS-CoV-2 cytopathic effect is blocked by lysosome alkalizing small molecules

Authors:
Kirill Gorshkov[1]*, Catherine Z. Chen[1], Robert Bostwick[2], Lynn Rasmussen[2], Bruce Nguyen Tran[1], Yu-Shan Cheng, Miao Xu[1], Manisha Pradhan[1], Mark Henderson[1], Wei Zhu[1], Eunkeu Oh[3], Kimihiro Susumu[3,4], Mason Wolak[3], Khalida Shamim[1], Wenwei Huang[1], Xin Hu[1], Min Shen[1], Carleen Klumpp-Thomas[1], Zina Itkin[1], Paul Shinn[1], Juan Carlos de la Torre[5], Anton Simeonov[1], Sam Michael[1], Matthew D. Hall[1], Donald C. Lo[1], Wei Zheng[1]*

Affiliations:

[1] National Center for Advancing Translational Sciences, 9800 Medical Center Drive, Rockville, MD, 20850, U.S.A.

[2] Southern Research Institute, 2000 Ninth Avenue South, Birmingham, Alabama, 35205, U.S.A.

[3]Optical Sciences Division, Code 5600, Naval Research Laboratory, Washington, D.C. 20375, U.S.A.

[4]Jacobs Corporation, Hanover, Maryland 21076, U.S.A.

[5] Department of Immunology and Microbiology, IMM6, The Scripps Research Institute, La Jolla, California 92037, U.S.A.

*To whom correspondence should be addressed:

Kirill Gorshkov – kirill.gorshkov@nih.gov
Wei Zheng – wzheng@mail.nih.gov

One Sentence Summary: SARS-CoV-2 infection and cytopathic effects can be blocked with lysosome alkalizing small molecules.

Supplementary Materials:

Supplementary Methods

Study Design

Sample Size and Replicates:

For the CPE, inter-plate duplicates were used for each data point for quantitative HTS and curve fitting. For CPE luminescence measurements, each well was read once. For the autophagy assay, three intra-plate replicates were used in consecutive columns for quantitative HTS, high-content analysis, and curve fitting. For the autophagy assay automated high-content imaging, each well was imaged 6 times in equally spaced fields using a 40x objective. This allowed for the collection of data from approximately 500 or more cells per well.

Data inclusion and outliers:

All data was included in the CPE assay. For the high-content imaging autophagy assays, efficacy data points were excluded in the case where there was >80% cell death. For non-linear curve fitting, data points were excluded when there was an experimental error that prevented proper drug addition or staining.

Selection of endpoints:

CPE assay 72 h and autophagy assay 16-18 h endpoints were selected *a priori* based on previous studies.

Research Objectives:

We aimed to contribute valuable pharmacological data towards the fight against COVID-19 by screening autophagy inhibitor compounds in a viral cytopathic effect assay to determine their potency and efficacy in preventing virally-induced cell death. We further aimed to validate these

autophagy inhibitors in a number of cell lines to understand whether the pharmacological effect of autophagy inhibition corresponded with anti-viral effects. Autophagy inhibition is a known anti-viral strategy effective *in vitro*, *in vivo*, and potentially in human patients. However, there is a lack of clinically available autophagy inhibitors due to dose-limiting adverse side effects. After screening, we identified a new preclinical compound ROC-325 is a potential target for further development.

Units of investigation:

Traditional cell culture methods were used in high-throughput formats for CPE and autophagy screening. Vero E6 cells previously developed by collaborators were used for the CPE assay. Vero E6, HEK293T, and HeLa cells were purchased from ATCC, and Huh-7.5 cells were a gift from the Tang Lab at FSU.

Experimental design:

The experiments put forth in this research article were controlled laboratory experiments devised with the guidelines established for high-throughput screening. Cells were maintained in a healthy state with proper cell culture techniques and treated using small volumes of compound dissolved in DMSO. Luminescence readings were collected for the CPE assay and fluorescence images were captured using automated high-content microscopy. Controls were assigned to specific wells and compounds were distributed throughout the entire 384 well plates. For the autophagy assays, compound dilutions were arranged vertically with the highest concentration in the middle of the plate and the lowest concentrations on the edges. Each compound was in three consecutive columns. Further details are provided in the Methods section. Measurements for the CPE assay

and fluorescence images were captured sequentially well by well. For the autophagy assay, a horizontal serpentine imaging sequence was used.

Blinding:

For the luminescence readings, the simple data structure was processed according to the plate layout annotation. For the autophagy assay, a custom high-content imaging protocol was developed in Columbus Analyzer for each cell line based on the detection of signals from the controls and the processing was automated. The data was initially processed using compound identifiers called NCGC values, and then the data was quantified and visualized in Excel and Prism GraphPad. The compound NCGC numbers were then unmasked using the corresponding compound names.

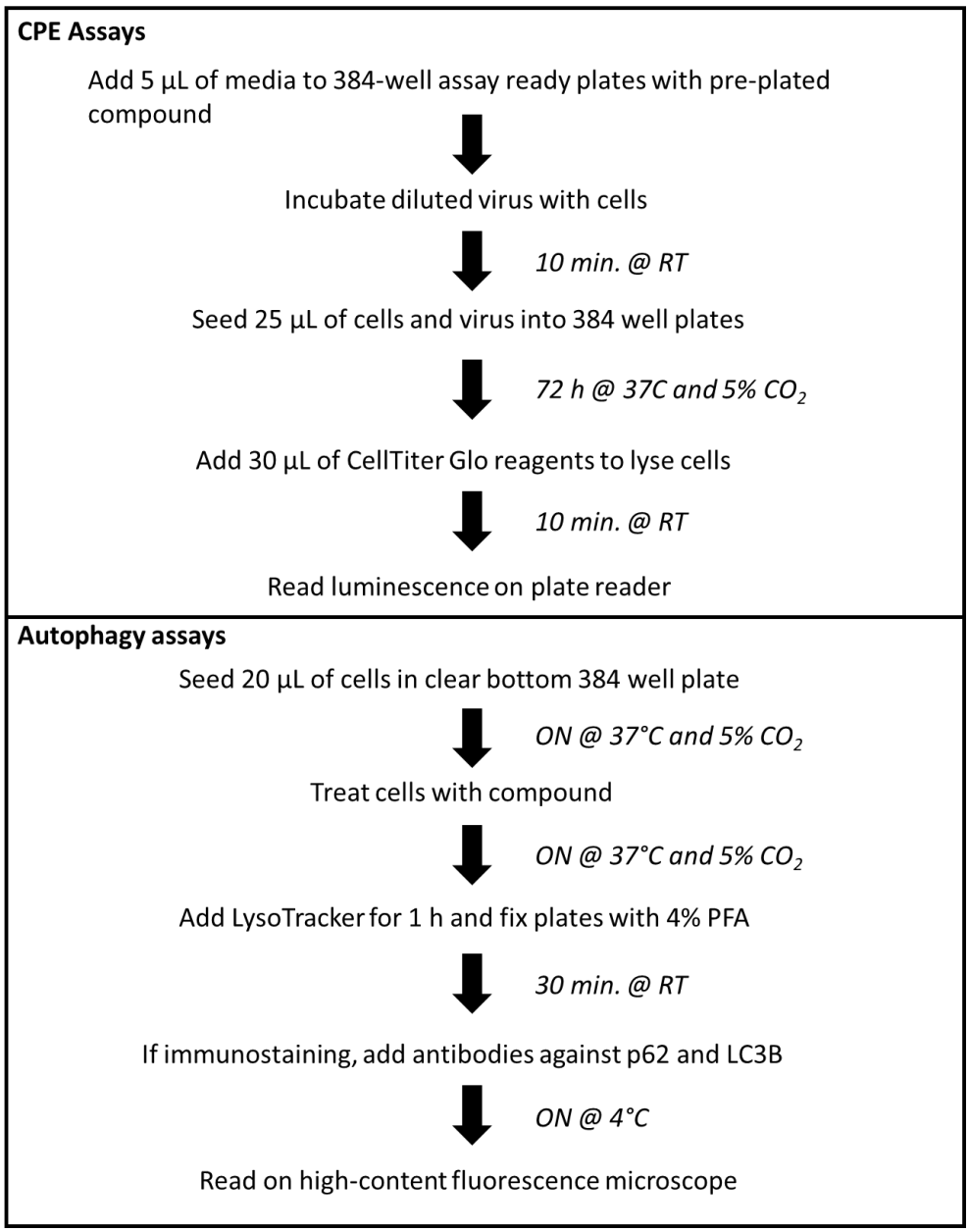

Fig. S1. Workflow overview for CPE and autophagy assays. Activities and incubation times are shown in a workflow.

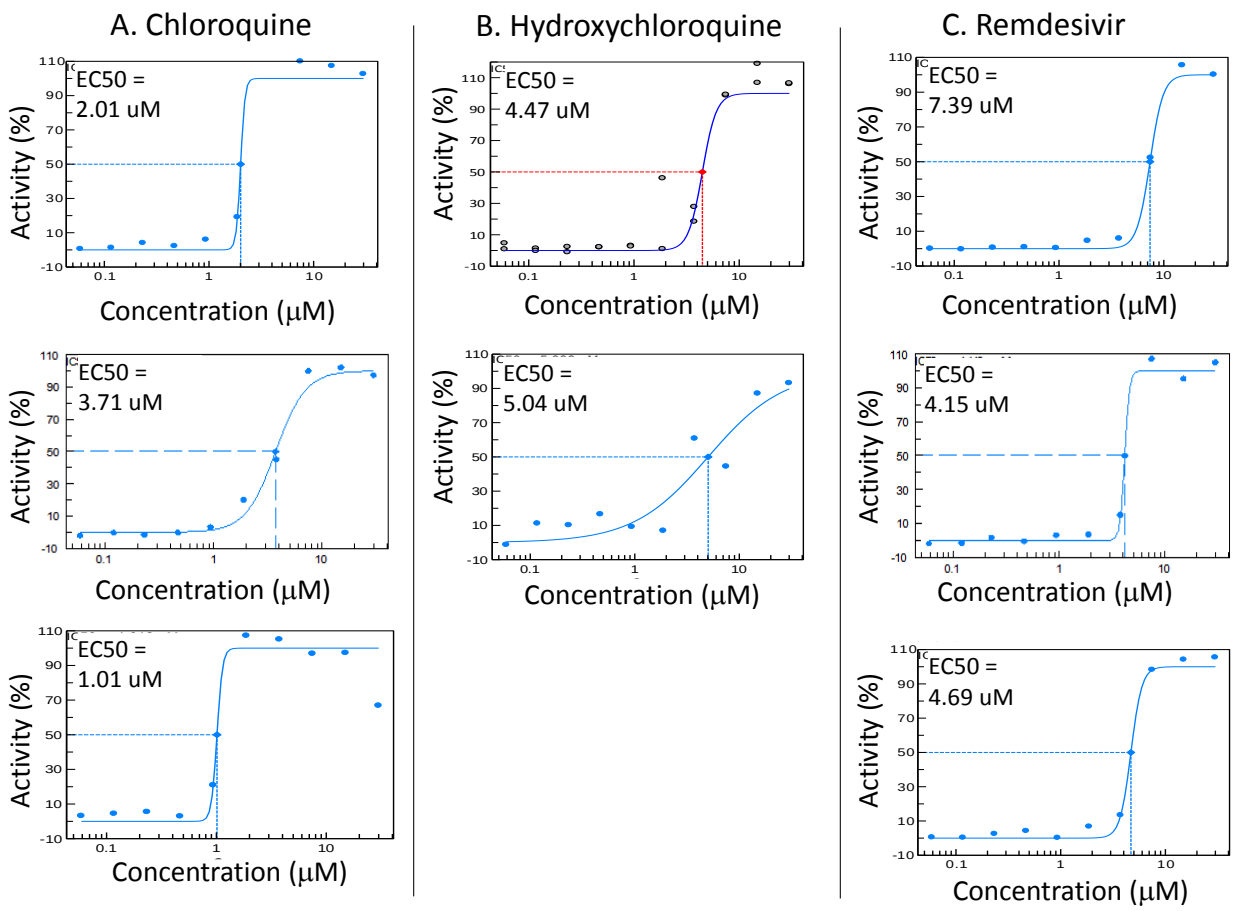

Fig. S2. CPE assay reproducibility. Compound concentration-response curves and EC50 values from experiments conducted on multiple dates are shown for (A) chloroquine, (B) hydroxychloroquine, and (C) remdesivir. The geometric mean EC50 is 1.96 μM for chloroquine, 4.75 μM for hydroxychloroquine, and 4.75 μM for remdesivir.

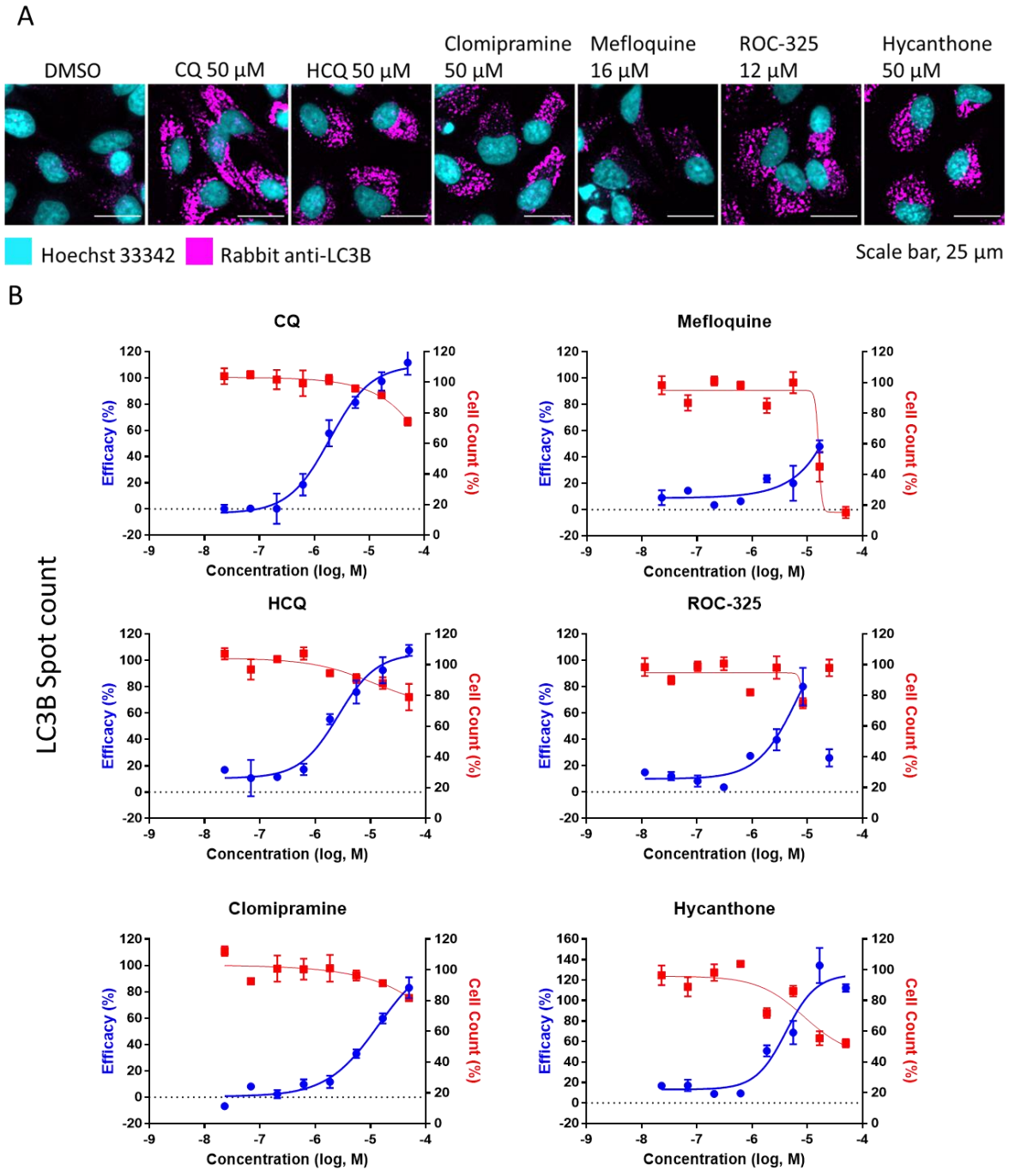

Fig. S3. Autophagy inhibition assay using LC3B immunostaining in HeLa cells. **(A)** Image montage of DMSO, CQ, HCQ, clomipramine, mefloquine, ROC-325, and hycanthone stained with Hoechst 33342 (cyan) and LC3B (magenta). CQ and HCQ images taken from wells in positive control column 2. Scale bar, 25 µm. **(B)** 8 point 1:3 dilution concentration-response

curves starting at 50 µM down to 0.023 µM for compounds in A. Blue curve indicates Efficacy, red curve indicates Cell Counts. Efficacy data normalized to DMSO (0%) and CQ (100%). Cell count data normalized to DMSO (100%) and 0 (no cells 0%). Error bars indicate SD. N=3 intra-plate replicates. Curves generated using non-linear regression.

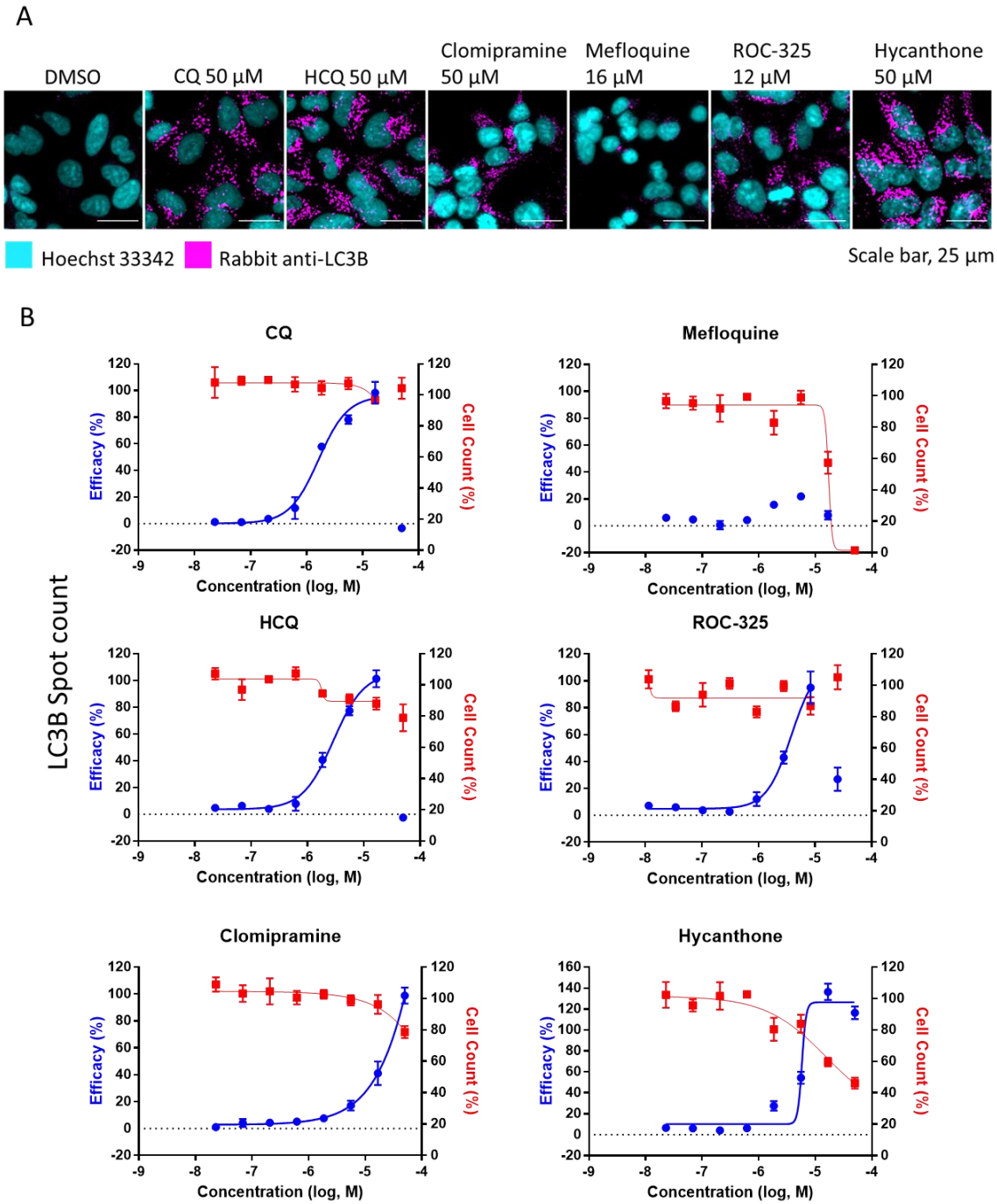

Fig. S4. Autophagy inhibition assay using LC3B immunostaining in HEK293T cells. **A)** Image montage of DMSO, CQ, HCQ, clomipramine, mefloquine, ROC-325, and hycanthone stained with Hoechst 33342 (cyan) and LC3B (magenta). CQ and HCQ images taken from wells in positive control column 2. Scale bar, 25 µm. **(B)** 8 point 1:3 dilution concentration-response

curves starting at 50 µM down to 0.023 µM for compounds in A. Blue curve indicates Efficacy, red curve indicates Cell Counts. Efficacy data normalized to DMSO (0%) and CQ (100%). Cell count data normalized to DMSO (100%) and 0 (no cells 0%). Error bars indicate SD. N=3 intra-plate replicates. Curves generated using non-linear regression.

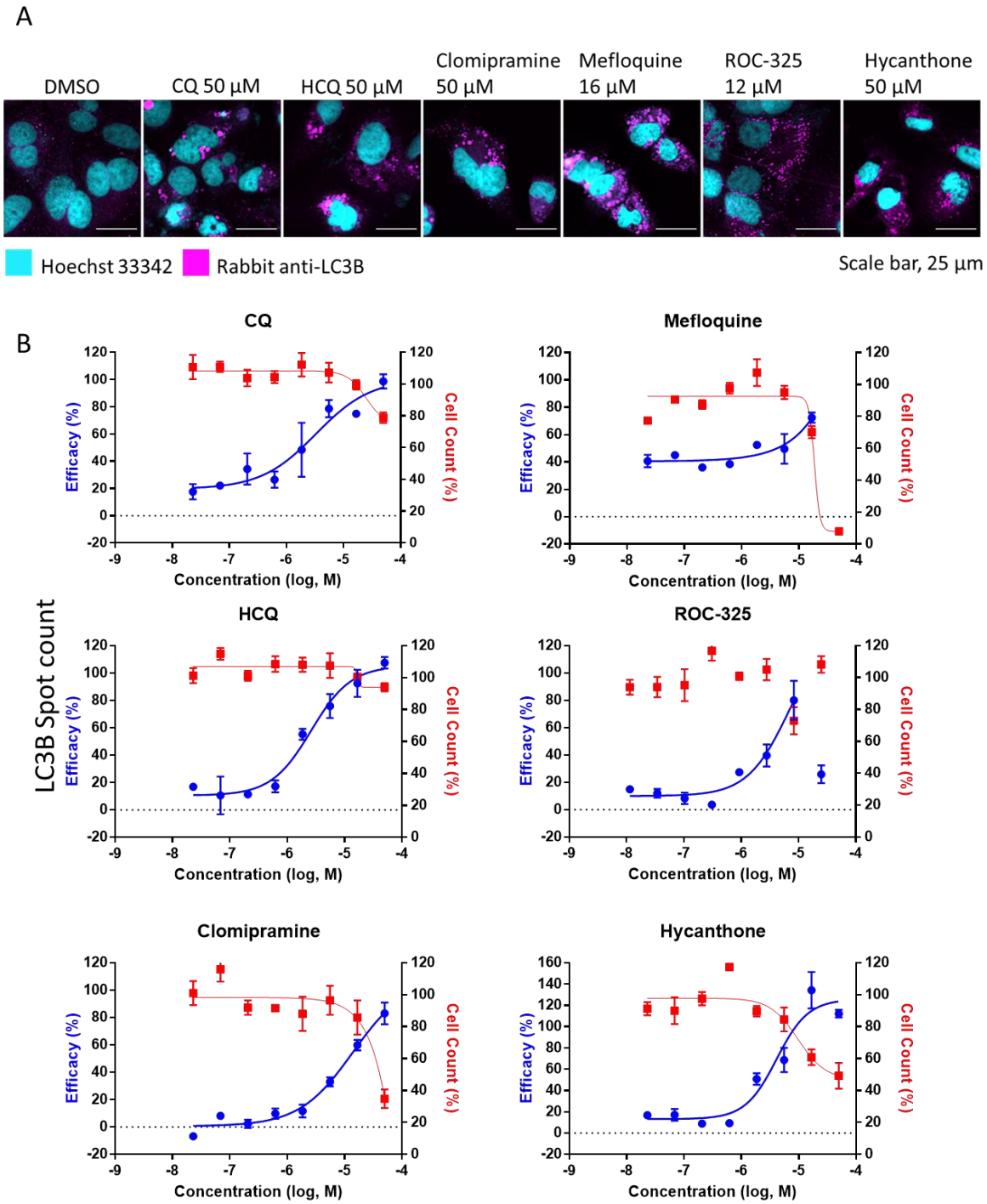

Fig. S5. Autophagy inhibition assay using LC3B immunostaining in Huh-7.5 cells. **(A)** Image montage of DMSO, CQ, HCQ, clomipramine, mefloquine, ROC-325, and hycanthone stained with Hoechst 33342 (cyan) and LC3B (magenta). CQ and HCQ images taken from wells in positive control column 2. Scale bar, 25 µm. **(B)** 8 point 1:3 dilution concentration-response

curves starting at 50 µM down to 0.023 µM for compounds in A. Blue curve indicates Efficacy, red curve indicates Cell Counts. Efficacy data normalized to DMSO (0%) and CQ (100%). Cell count data normalized to DMSO (100%) and 0 (no cells 0%). Error bars indicate SD. N=3 intra-plate replicates. Curves generated using non-linear regression.

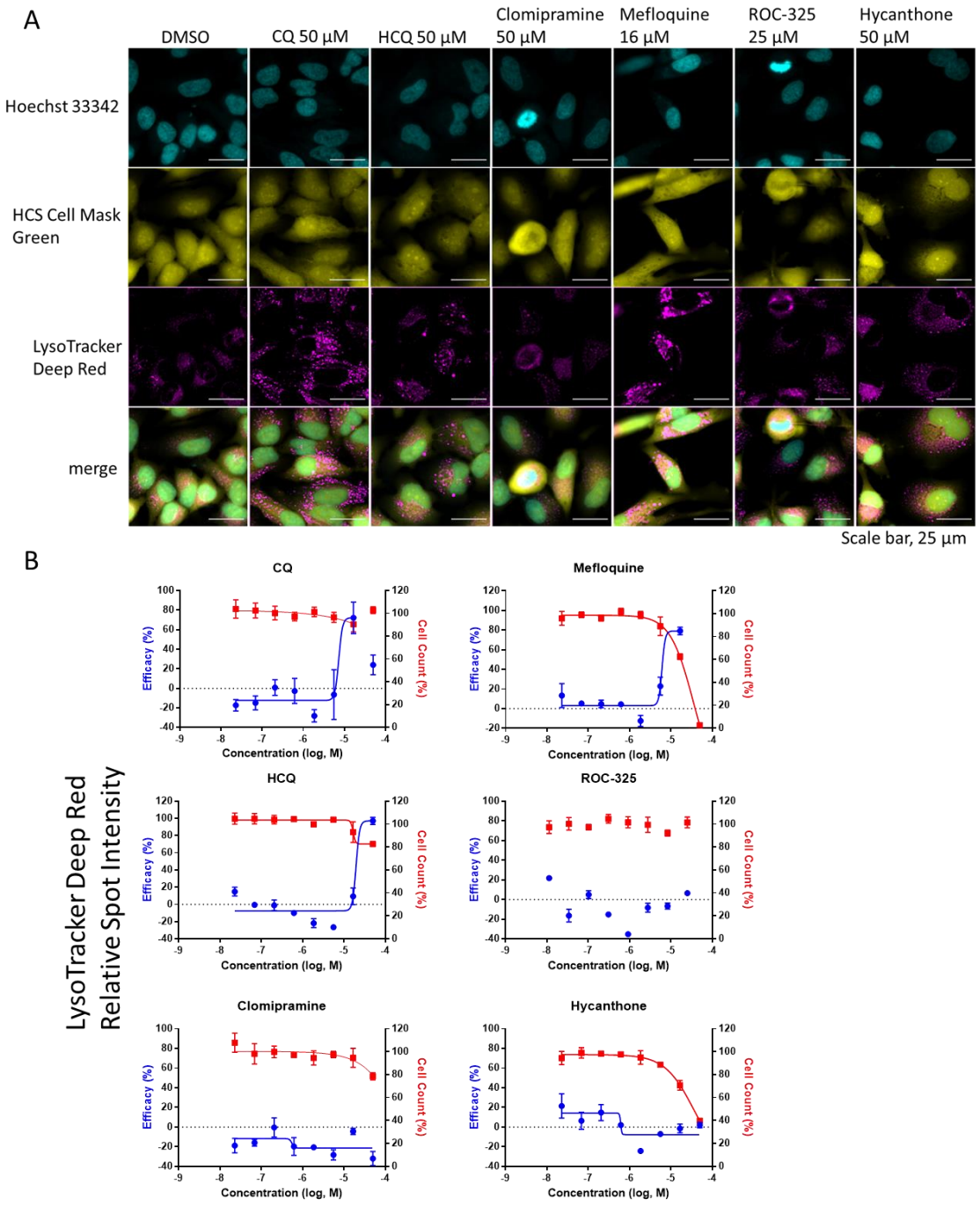

Fig. S6. LysoTracker Deep Red staining in HeLa cells. **(A)** Image montage of DMSO, CQ, HCQ, clomipramine, mefloquine, ROC-325, and hycanthone stained with Hoechst 33342 (cyan), HCS Cell Mask Green (yellow), and LysoTracker Deep Red (magenta). CQ and HCQ images taken from wells in positive control column 2. Scale bar, 25 µm. **(B)** 8 point 1:3 dilution

concentration-response curves starting at 50 µM down to 0.023 µM for compounds in A. Blue curve indicates Efficacy, red curve indicates Cell Counts. Efficacy data normalized to DMSO (0%) and CQ (100%). Cell count data normalized to DMSO (100%) and 0 (no cells 0%). Error bars indicate SD. N=3 intra-plate replicates. Curves generated using non-linear regression.

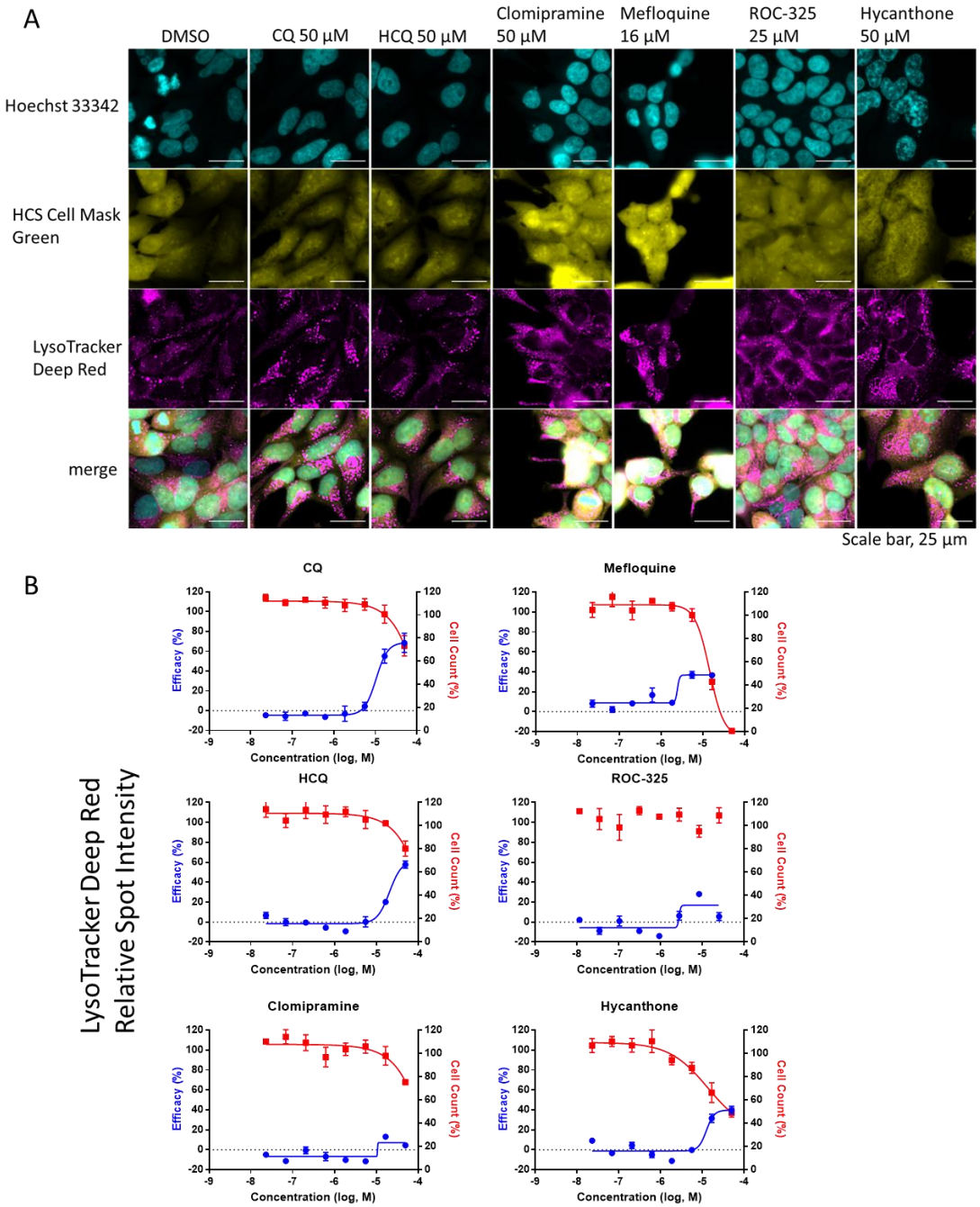

Fig S7. LysoTracker Deep Red staining in HEK293T cells. **(A)** Image montage of DMSO, CQ, HCQ, clomipramine, mefloquine, ROC-325, and hycanthone stained with Hoechst 33342 (cyan), HCS Cell Mask Green (yellow), and LysoTracker Deep Red (magenta). CQ and HCQ images taken from wells in positive control column 2. Scale bar, 25 µm. **(B)** 8 point 1:3 dilution concentration-response curves starting at 50 µM down to 0.023 µM for compounds in A. Blue curve indicates Efficacy, red curve indicates Cell Counts. Efficacy data normalized to DMSO (0%) and CQ (100%). Cell count data normalized to DMSO (100%) and 0 (no cells 0%). Error bars indicate SD. N=3 intra-plate replicates. Curves generated using non-linear regression.

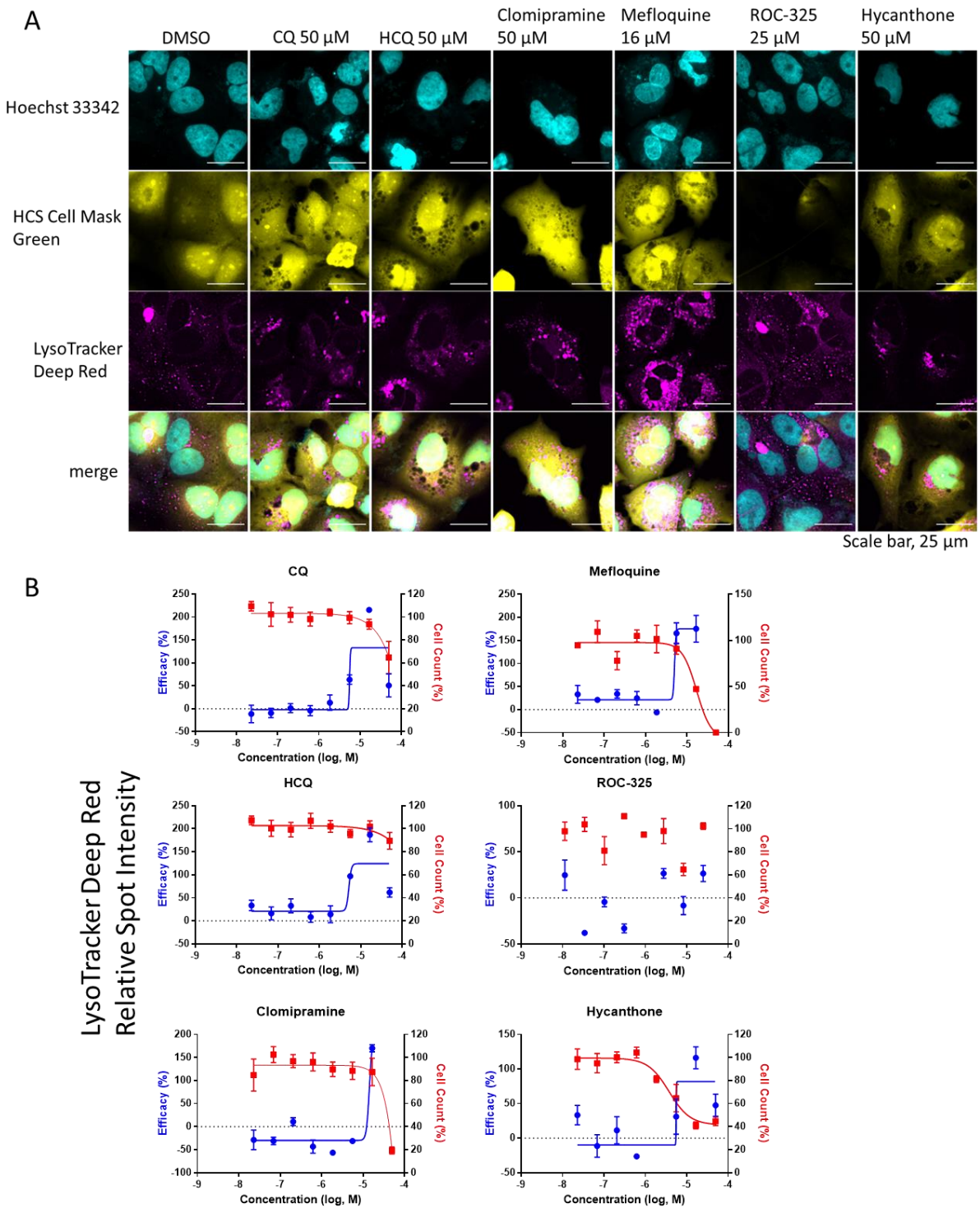

Fig S8. LysoTracker Deep Red staining in Huh-7.5 cells. **(A)** Image montage of DMSO, CQ, HCQ, clomipramine, mefloquine, ROC-325, and hycanthone stained with Hoechst 33342 (cyan), HCS Cell Mask Green (yellow), and LysoTracker Deep Red (magenta). CQ and HCQ images

taken from wells in positive control column 2. Scale bar, 25 µm. **(B)** 8 point 1:3 dilution concentration-response curves starting at 50 µM down to 0.023 µM nM for compounds in A. Blue curve indicates Efficacy, red curve indicates Cell Counts. Efficacy data normalized to DMSO (0%) and CQ (100%). Cell count data normalized to DMSO (100%) and 0 (no cells 0%). Error bars indicate SD. N=3 intra-plate replicates. Curves generated using non-linear regression.

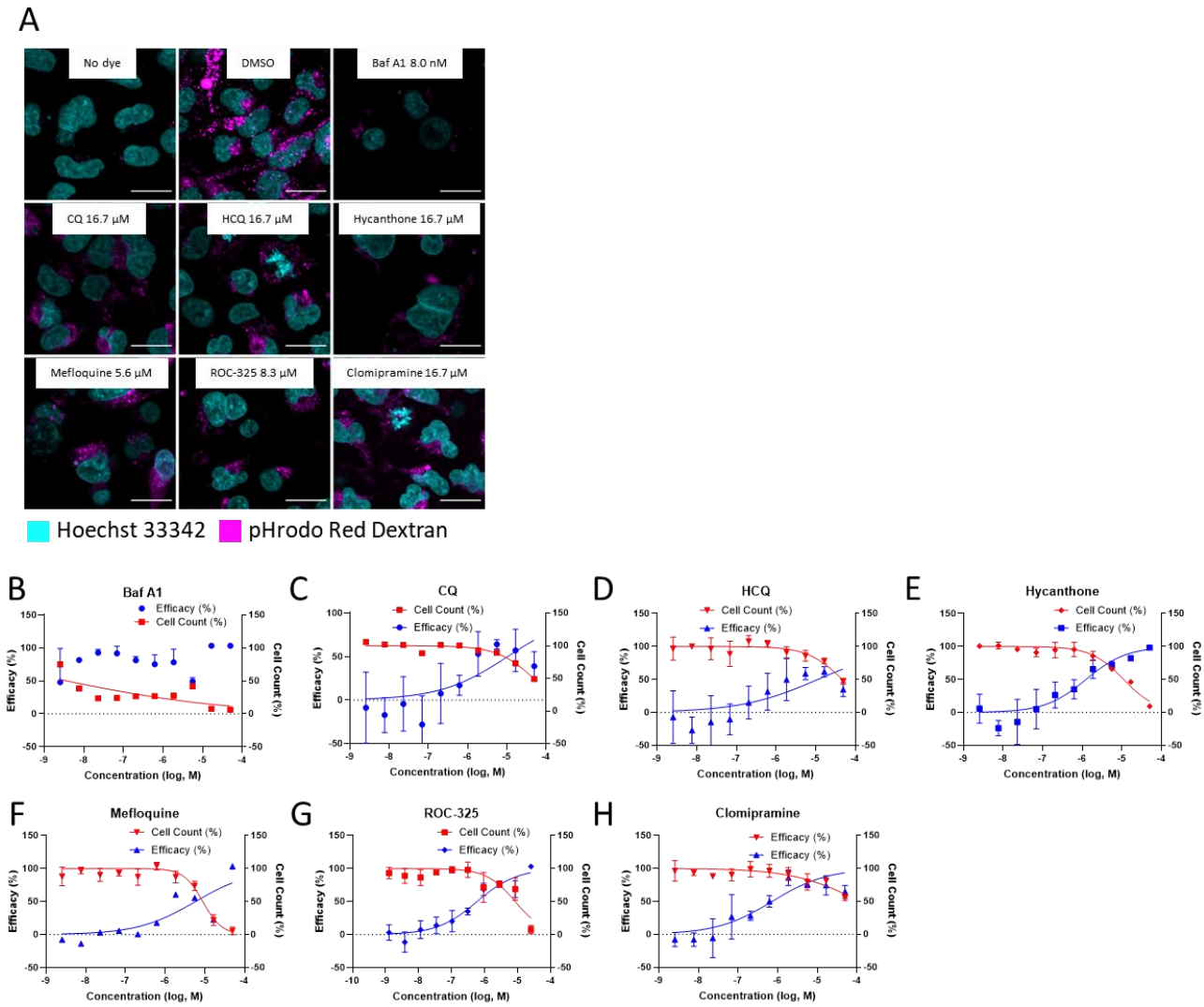

Fig. S9 Compounds inhibit pHrodo Red Dextran uptake in ACE2-GFP HEK293T cells. **(A)** Confocal images of cells treated with compounds for 48 h and stained with Hoechst (cyan) and pHrodo Red Dextran (magenta). Scale bar, 20 µm. Activity and cytotoxicity curves for **(B)** Bafilomycin A1, **(C)** CQ, **(D)** HCQ, **(E)** Hycanthone, **(F)** Mefloquine, **(G)** ROC-325, and **(H)** Clomipramine treated ACE2-GFP HEK293T cells for 48 h followed by 30 min. pHrodo Red Dextran uptake. Curves generated using non-linear regression. N=triplicate wells from a 384 well plate,

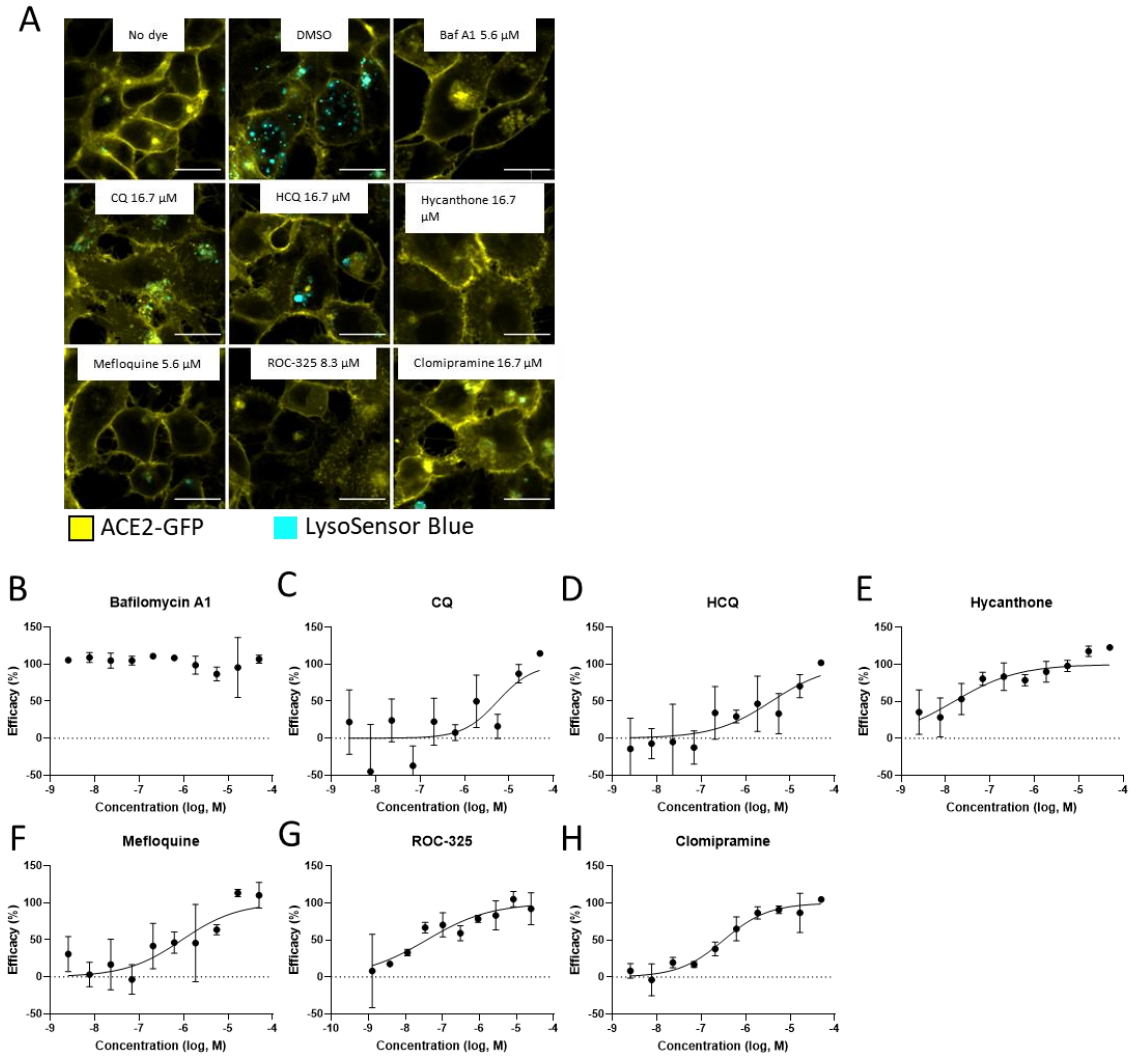

Fig. S10 Compounds inhibit LysoSensor Blue staining in ACE2-GFP HEK293T cells. **(A)** Confocal images of cells treated with compounds for 48h and stained with LysoSensor Blue (cyan) and stably expressed ACE2-GFP (yellow). Scale bar, 20 µm. Activity curves for **(B)** Bafilomycin A1, **(C)** CQ, **(D)** HCQ, **(E)** Hycanthone, **(F)** Mefloquine, **(G)** ROC-325, and **(H)** Clomipramine treated ACE2-GFP HEK293T cells for 48 h followed by 30 min. LysoSensor Blue treatment. Curves generated using non-linear regression. N=triplicate wells from a 384 well plate (305±66 cells per well from two fields).

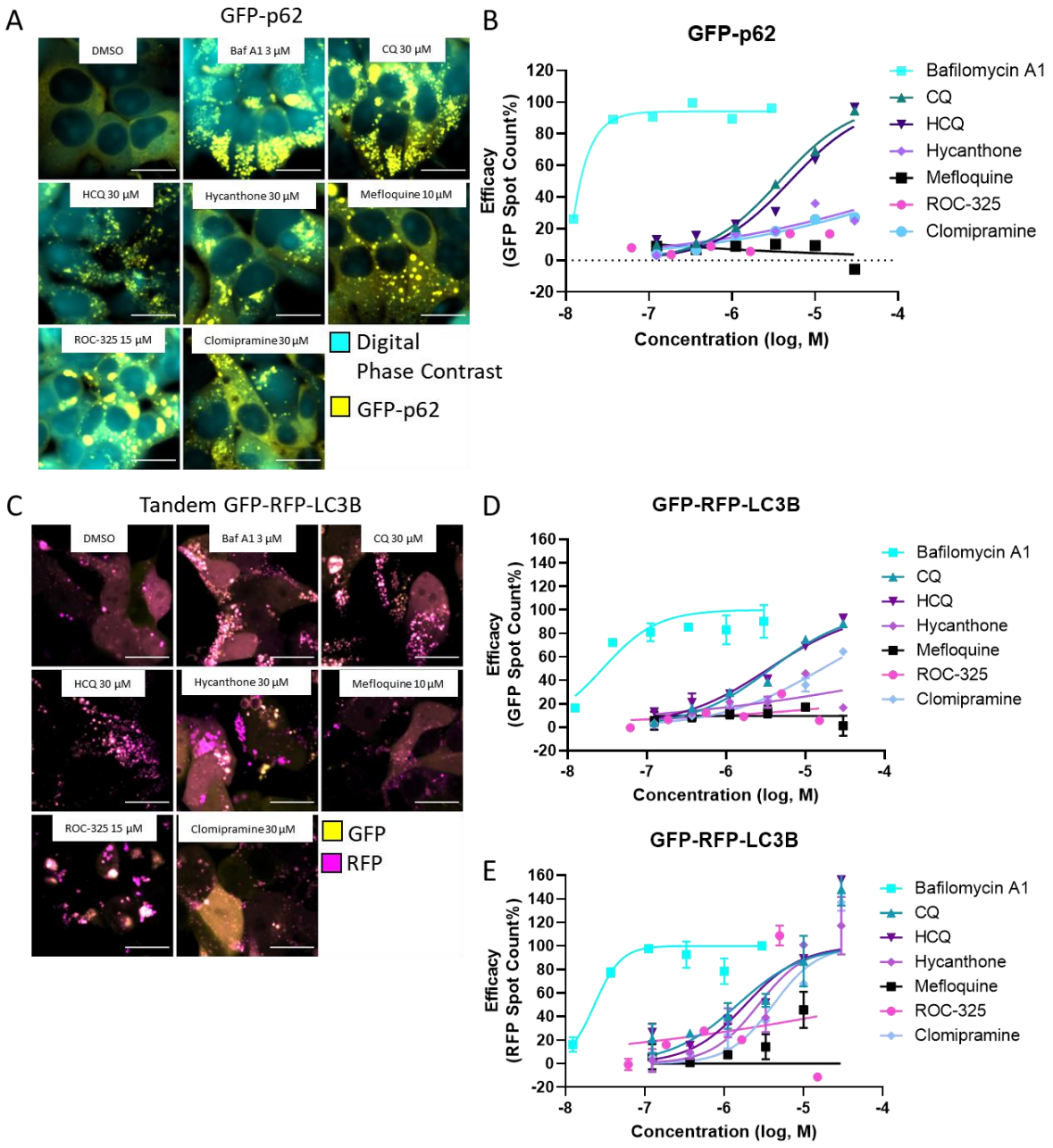

Fig. S11 Compounds induce accumulation of p62 and LC3B. **(A)** Confocal images of cells transduced with Bacmam 2.0 GFP-p62 probe (yellow) treated with compounds for 16 h and transduced with. Digital phase contrast used to identify cell bodies. Scale bar, 20 µm. **(B)** Activity curves for Bafilomycin A1 (cyan), CQ (teal), HCQ (dark purple), Hycanthone (light purple), Mefloquine (black), ROC-325 (pink), and Clomipramine (light blue) treated ACE2-GFP

HEK293T cells for 16 h after 40 h transduction with Bacmam 2.0 GFP-p62. N=one well from a 96 well plate (369±44 cells from five fields). **(C)** Confocal images of cells treated with compounds for 16 h and stained with Hoechst (cyan) and transduced with Bacmam 2.0 GFP-RFP-LC3B probe (GFP yellow/RFP magenta). **(D)** Activity curves for Bafilomycin A1 (cyan), CQ (teal), HCQ (dark purple), Hycanthone (light purple), Mefloquine (black), ROC-325 (pink), and Clomipramine (light blue) for cells in C. Curves generated using non-linear regression Scale bar, 20 μm.

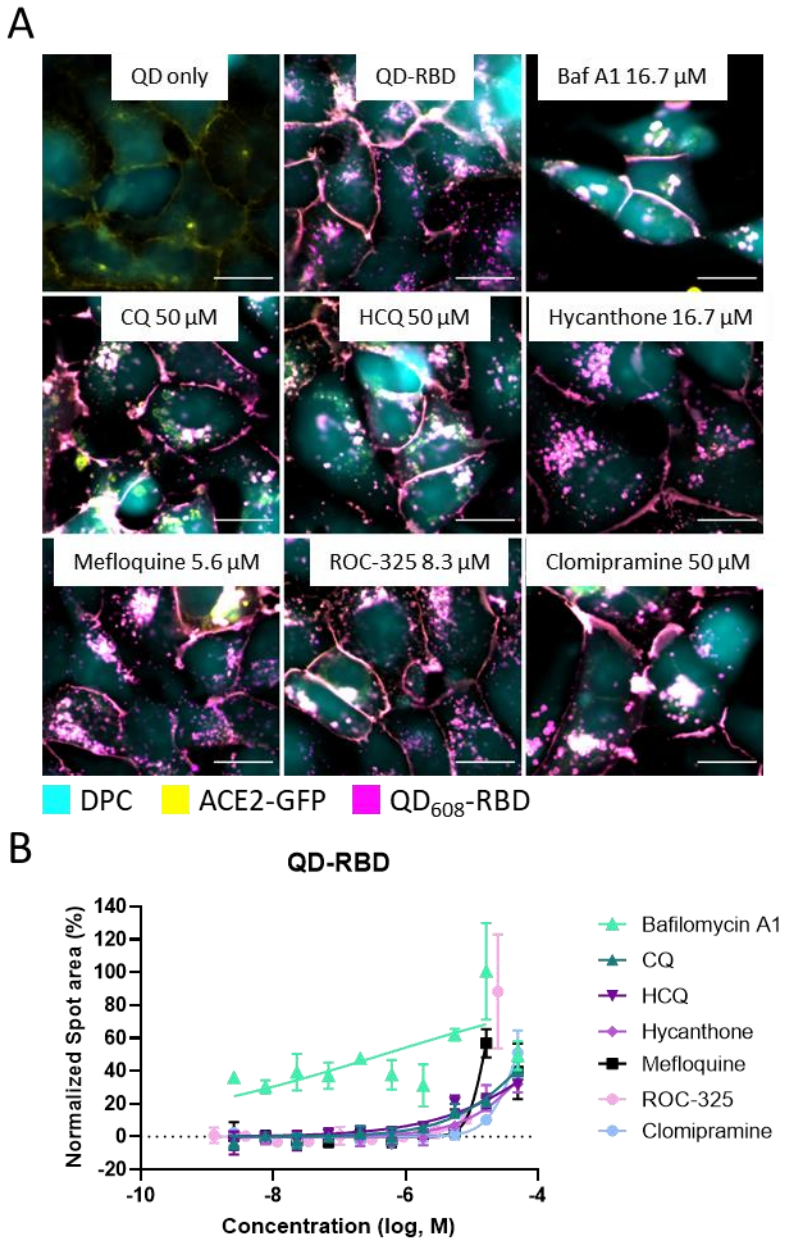

Fig. S12 Compounds do not block quantum dot-conjugated SARS-CoV-2 receptor binding domain (RBD) from entering cells, but do increase size of QD-RBD puncta. **(A)** Confocal images of ACE2-GFP (yellow) cells treated with compounds for 24h followed by three hour incubation with quantum dot-conjugated SARS-CoV-2 RBD (magenta). Digital Phase Contrast used to visualize cell bodies. Scale bar, 20 µm. **(B)** Activity curves for Bafilomycin A1 (cyan), CQ (teal), HCQ (dark purple), Hycanthone (light purple), Mefloquine (black), ROC-325 (pink),

and Clomipramine (light blue). Curves generated using non-linear regression. N=triplicate wells from a 384 well plate (351±50 cells per well from three fields).

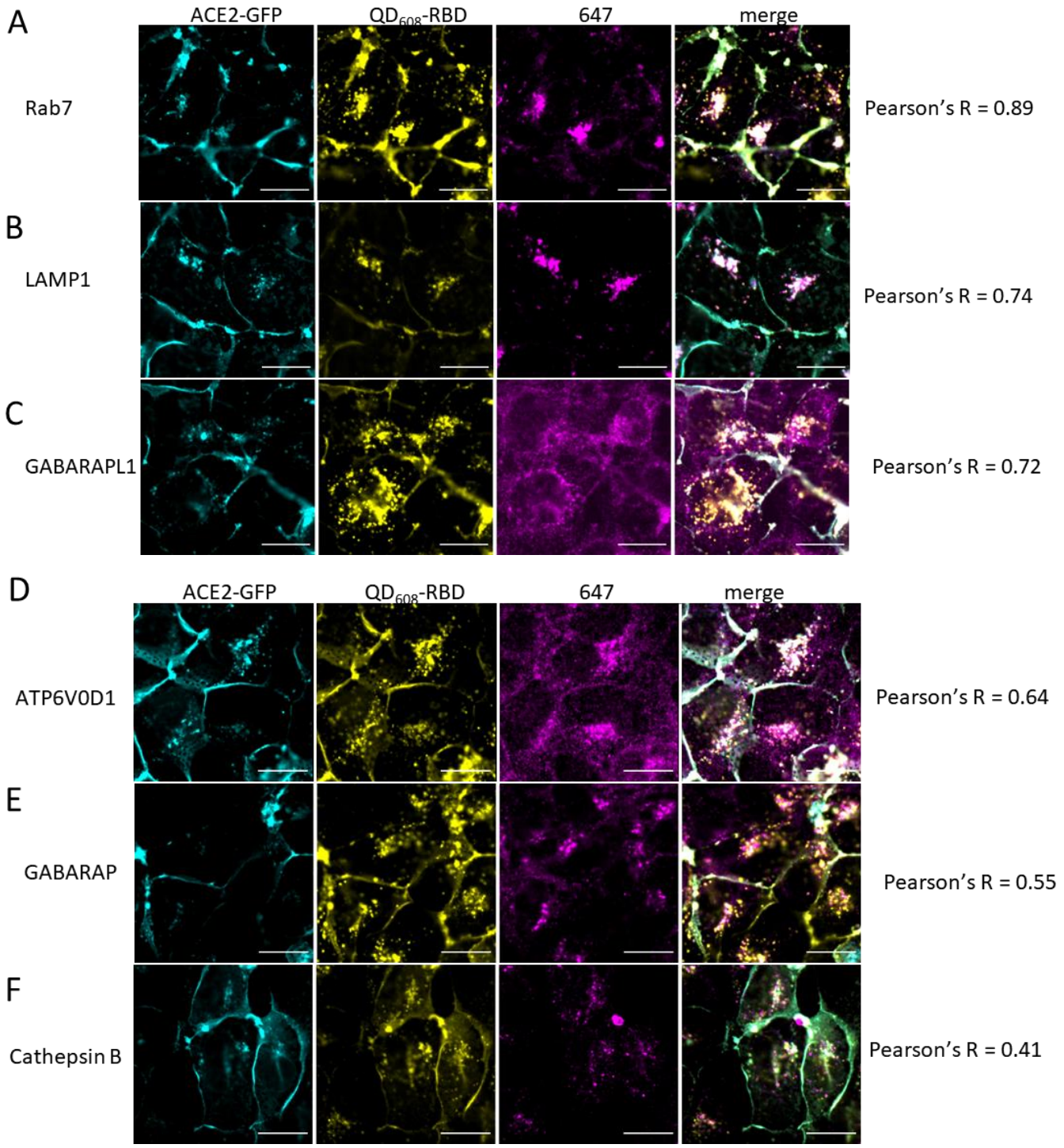

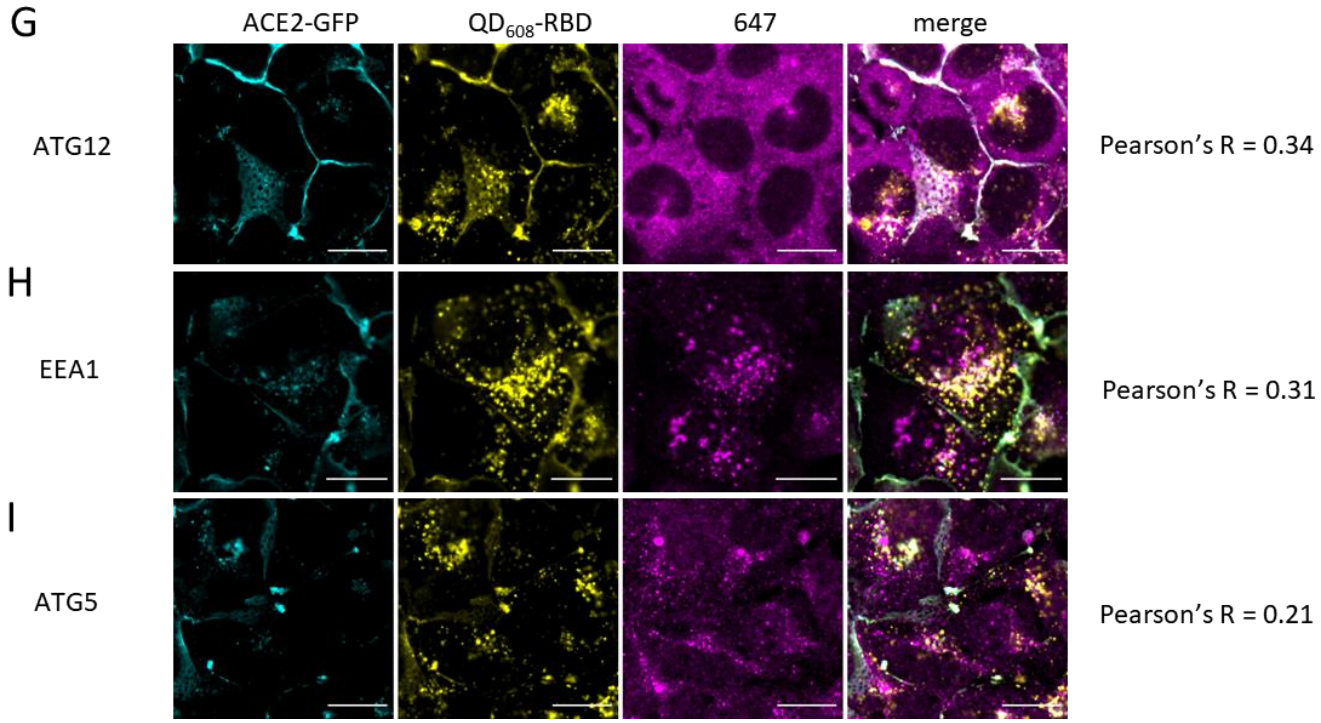

Fig. S13 QD-RBD colocalizes with endosomal and lysosomal markers. Confocal images of ACE2-GFP (yellow) cells treated with QD-RBD (magenta) and immunostained for markers **(A)** Rab7, **(B)** LAMP1, **(C)** GABARAPL1, **(D)** ATP6V0D1, **(E)** GABARAP, **(F)** Cathepsin B, **(G)** ATG12, **(H)** EEA1, **(I)** ATG5. Pearson's R value shown for the field of view in each panel to measure colocalization of QD-RBD and the protein of interest. Scale bar, 20 μm. Cells shown are representative of three wells from a 96-well plate.

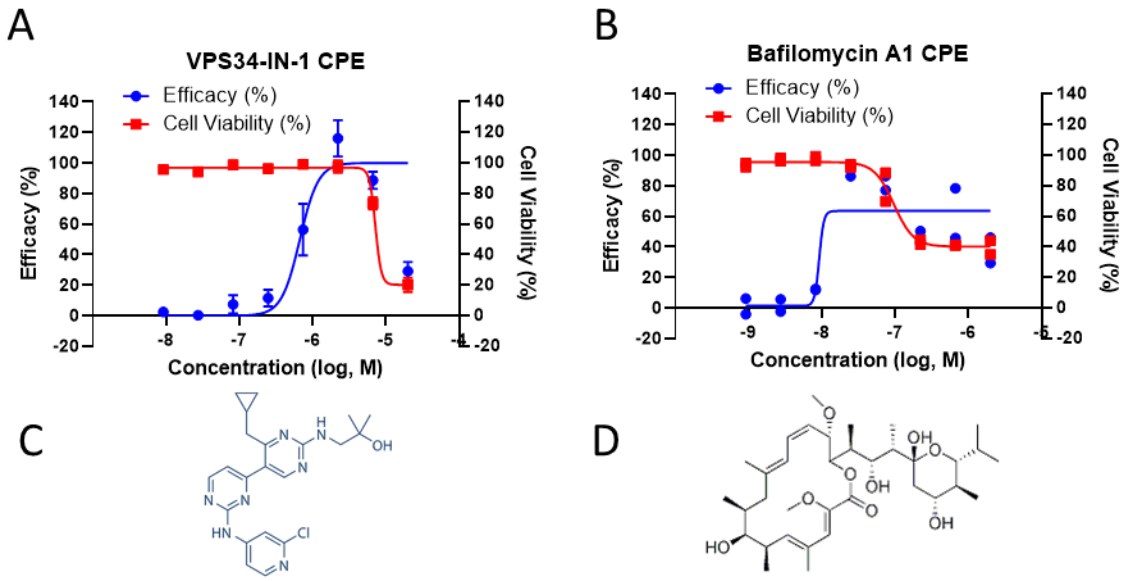

Fig. S14 Endosomal trafficking inhibitor VPS34-IN-1 and Bafilomycin A1 prevent the SARS-CoV-2 cytopathic effect in Vero E6 cells. Activity and Cell Viability curves for **(A)** VPS34-IN1 (N=triplicate wells from a 384-well plate) and **(B)** Bafilomycin A1 (N=duplicate wells from a 384 well plate). Curves generated using nonlinear regression. **(C)** Structure of VPS34-IN-1. **(D)** Structure of Bafilomycin A1.

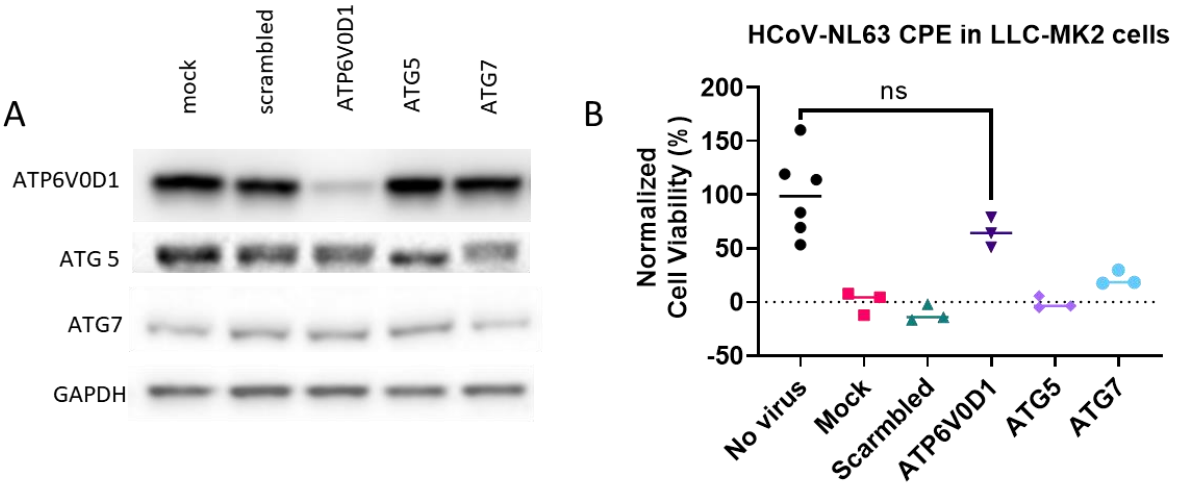

Fig. S15 LLC-MK2 cells are protected from HCoV-NL63 CPE after siRNA knockdown of ATP6V0D1. **(A)** Western blot of ATP6V0D1, ATG5, and ATG7 from LLC-MK2 cells treated with siRNA against the indicated proteins. GAPDH used as loading control. **(B)** Cell viability (%) as measured by ATPlite reagent of LLC-MK2 cells transfected with siRNA for 48 h followed by infection by HCoV-NL63 for 72 h to induce CPE. N=three wells from a 96-well plate.

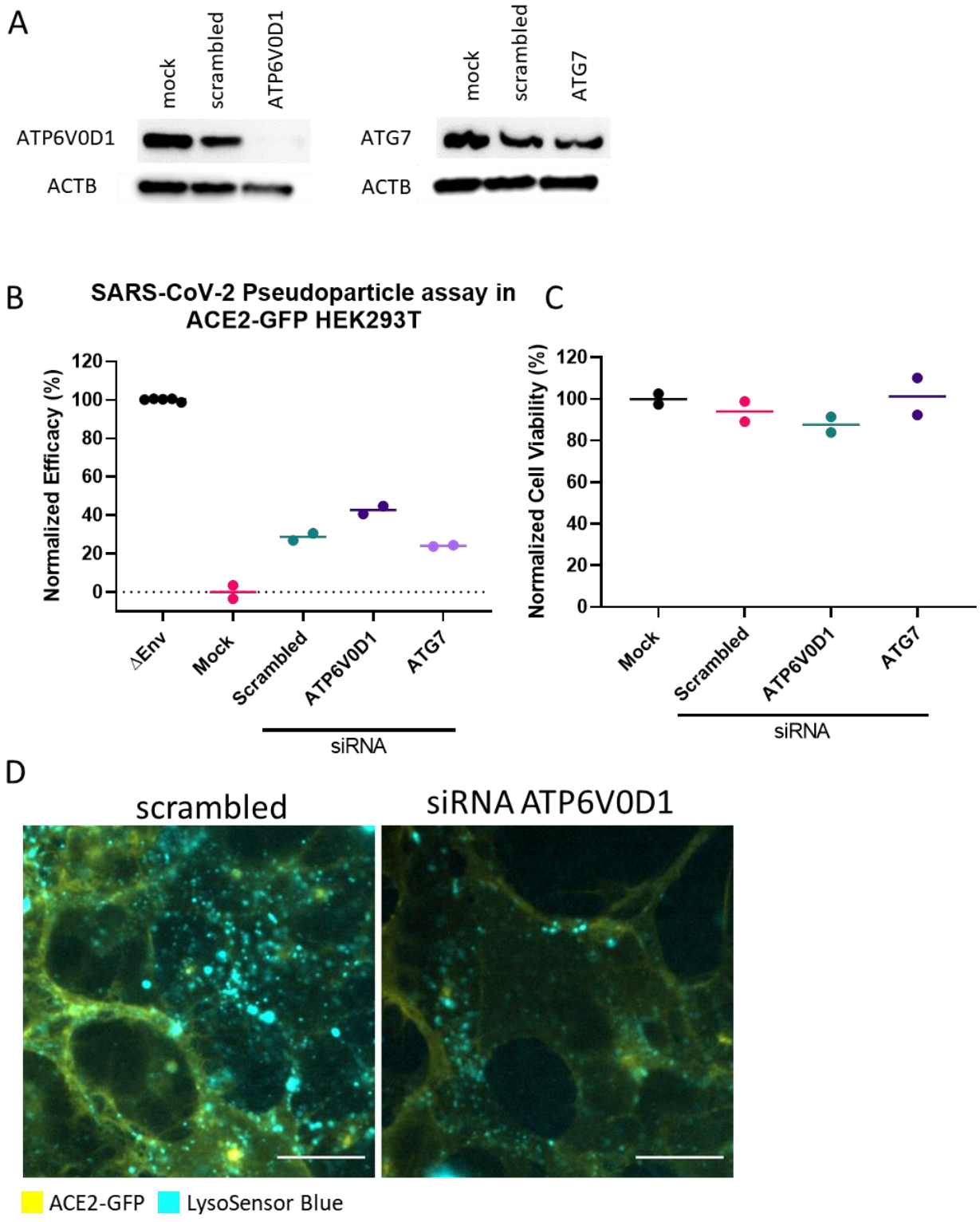

Fig. S16 ATP6V0D1knockdown partially blocks SARS-CoV-2 PP transduction in ACE2-GFP HEK293T cells. **(A)** Western blot of ACE2-GFP HEK293T cells transfected for 48 h with

siRNA against mock, scrambled control, ATP6V0D1 and ATG7. **(B)** Inhibition measurements of SARS-CoV-2 PP transduction of siRNA transfected ACE2-GFP HEK293T cells. Data normalized to delEnv (100%) and mock (0%). N=duplicate wells from a 96-well plate. **(C)** Cell viability of siRNA transfected ACE2-GFP HEK293T cells. Data normalized to mock (100%) and media containing no cells (0%). N=duplicate wells from a 96-well plate. **(D)** Representative images of live ACE2-GFP cells stained with LysoSensor Blue after 48 h of siRNA transfection to knockdown ATP6V0D1. Scale bar, 20 μm.